

D. RUNDE
S. BRUNKEN
S. BREUER
D. KIP[✉]

Integrated-optical add/drop multiplexer for DWDM in lithium niobate

Institute of Physics and Physical Technologies, Clausthal University of Technology, Leibnizstrasse 4, 38678 Clausthal-Zellerfeld, Germany

Received: 17 January 2007/Revised version: 30 March 2007
Published online: 22 May 2007 • © Springer-Verlag 2007

ABSTRACT In this contribution, an add/drop multiplexer that uses a mode-selective coupler and a holographically recorded slanted Bragg grating in lithium niobate is demonstrated. A Bragg grating with a bandwidth of 0.1 nm allows for an add/drop efficiency of about 96% with a cross-talk well above 22 dB applicable for wavelengths in the 1.5 μm window. Polarisation-independent operation can be achieved by application of a bias electric field to compensate for the small mismatch of propagation constants of TE and TM modes. The proposed scheme of an integrated-optical lithium niobate based device appears to be an interesting option due to its potential for fast electro-optical switching.

PACS 42.40.Ht; 42.65.Hw; 42.70.Ln; 42.82.Cr; 42.82.Et

1 Introduction

The consistently increasing volume of data transferred through optical networks has led to the development of more advanced technologies like dense wavelength division multiplexing (DWDM) [1]. In DWDM, each communication channel allocates a different wavelength that is multiplexed onto a single optical fibre, which allows for utilizing the high optical carrier bandwidth to a greater extent. In nodes of DWDM networks, so-called add/drop multiplexers are utilized to either add or drop certain channels into and out of an optical fibre line. In the last decade, several different multiplexer concepts for add/drop operation have been proposed. These include fibre Bragg gratings (FBG) in conjunction with circulators [2, 3], thin film optical filters, arrayed waveguide gratings [4], and grating-assisted Mach–Zehnder interferometers [5], to name only a few. Fibre-based add/drop multiplexers for DWDM without the need for an additional circulator have been proposed and realized using tapered fibres and UV recorded FBG's in germanium-doped quartz fibres [6–8]. In such devices, a tilted Bragg grating reflects a certain wavelength channel out of an input multi-channel data stream to a drop channel. Spatial separation of the reflected signal from the input is realized by a mode-selective directional coupler.

Because it has been recognized that these fibre-based devices can hardly be realized with high yield for mass fabrication, the same concept has later been transferred to planar geometries with much lower fabrication tolerances due to precise lithographic patterning in glasses and polymers [9–11].

In this contribution, we report on an integrated-optical add/drop multiplexer that uses holographically recorded Bragg gratings and two mode-selective couplers in electro-optic lithium niobate (LiNbO_3) [12, 13]. Bragg gratings yield high reflection efficiency and tailored spectral bandwidths, and integrated optics make possible compact, light-weight, and electrically tuneable and switchable devices. The feasibility of the proposed multiplexer for application in DWDM networks in the 1.5 μm wavelength range is experimentally investigated, showing high filter efficiency, small bandwidth and low cross-talk. Finally, by using the electro-optic properties of a LiNbO_3 based device, we show the general suitability of this device for fast electrical switching and wavelength tuning.

2 Principle of operation

The scheme of our device is depicted in Fig. 1. A multi-wavelength signal inserted at the input port S_{in} excites the fundamental mode of a single-mode channel waveguide. This light passes the taper region and is adiabatically converted to the fundamental mode of the central bi-modal waveguide section, where it unaffectedly passes a mode-selective coupler. This mode-selective coupler is designed to evanescently couple only the first higher mode of the bi-modal waveguide to the fundamental mode of a parallel, single-mode channel. In the central bi-modal region, non-resonant wavelength channels that do not fulfil the Bragg condition will propagate to the output port S_{out} and pass the device. On the other hand, a resonant wavelength channel gets Bragg reflected at the holographic grating and is thereby converted into the backward-propagating first higher mode because of the tilt of the grating. For this higher mode, the directional coupler is resonant and extracts the reflected signal to the drop port D. Here a standard s-bend allows for the required spatial separation of ports to use commercial v-grooves for fibre interconnection. In case of a small fraction of remaining intensity of backward-propagating light of the higher mode, this light will be radiated off at the entrance of the taper sec-

✉ Fax: +49-5323-722175, E-mail: d.kip@pe.tu-clausthal.de

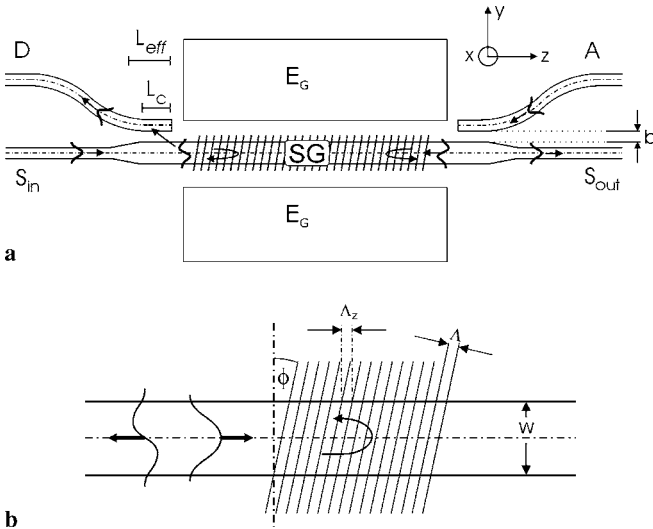


FIGURE 1 (a) Scheme of the add/drop multiplexer. S_{in} , single-mode input port; D, drop port; A, add port; S_{out} , single-mode output port; SG, slanted grating in bi-modal waveguide section; E_G , coplanar electrodes; L_C , L_{eff} , coupler length (parallel waveguide section) and total effective coupling length; b , inter-waveguide distance. (b) Mode conversion by the tilted grating. The fundamental mode of resonant wavelength λ_B is converted by the Bragg grating into the backwards propagating first higher mode. w , waveguide width; Λ , grating period; Λ_z , effective grating period; φ , tilt angle

tion. The reverse function of the coupler is used to realize the add operation in a symmetric layout on the right hand side of Fig. 1. To achieve this, an optical channel with appropriate wavelength is coupled into the add port A, transformed to the higher mode of the bi-modal waveguide via the mode-selective coupler, gets Bragg reflected and thereby converted to the fundamental mode at the grating, and finally leaves the device at the output port S_{out} .

The Bragg wavelength of the grating can be continuously altered by using the electro-optic effect in LiNbO₃ crystals. This is realized by applying an electric field to the grating section with the help of coplanar electrodes E_G . On one hand, applying a voltage to the electrodes allows for fast electrical on/off switching of a single channel with time constants in the microsecond regime and below. On the other hand, because of the inherent asymmetric shape of the used channel waveguide, the propagation constants of TE and TM polarised modes may slightly differ, thus leading to slightly different individual Bragg wavelengths of the two polarisation components of a non-polarised input signal. To compensate for this difference in wavelength, a bias electric field can be used, which makes use of the fact that the relevant electro-optic tensor elements have opposite signs for TE and TM polarisation. In this way, a polarisation-independent operation of the device may be achieved.

3 Device modelling

In a recently submitted manuscript, we have investigated the mode-selective coupler used here for the add/drop multiplexer in detail [13]. After systematic numerical modelling using finite-difference and beam propagation methods, optimized parameters for the waveguide widths, taper section, s-bends, waveguide distance, and coupler lengths were

found. Based on these investigations, in the same work we experimentally demonstrated a mode-selective coupler with a maximum efficiency of above 90% using 6 μm and 12 μm wide channels for single- and two-mode waveguides, respectively, a 1.5 mm long taper section, s-bends with a length of 10 mm for a separation of 127 μm of input and output ports, an inter-waveguide distance of 4.5 μm and a coupler length L_C (parallel waveguide section) of 0.25 mm, which resulted in an effective coupling length of about 1.3 mm [13]. The same parameters (only an inter-waveguide distance of 5 μm is used instead of 4.5 μm) were used here to fabricate the add/drop multiplexer. In order to record gratings with high diffraction efficiency, the length of the bi-modal waveguide section is set to 20 mm. With typical photorefractive refractive index amplitudes Δn of the order of 10^{-4} for ordinarily polarised light, a reflectivity close to 100% may be obtained. Nevertheless, higher reflectivities may be obtained using longer gratings and/or stronger doping, allowing for larger refractive index changes.

For a high efficiency and a low cross-talk of the add/drop multiplexer, a tilted Bragg grating for effective mode conversion of the fundamental mode to the backward-propagating next higher mode and vice versa is required. At the same time, a simple reflection of the fundamental mode alone as well as a reflection of the first higher mode without mode conversion should be minimized. It has already been shown that the fabrication of such gratings can be realized by using two-beam interference in photorefractive LiNbO₃ channel waveguides [12, 14]. Alternatively, the use of adequate phase masks may provide an increased stability of the recording set-up. For long-term stability, the Bragg gratings can be thermally fixed by recording at elevated temperatures around 160 °C [15, 16]. The coupling efficiency of our Bragg grating can be calculated using the overlap integral Q of the two modes [10]

$$Q(\varphi) = \frac{\iint E_1(x, y)\varepsilon(y, \varphi)E_0(x, y, \varphi) dx dy}{\sqrt{\iint |E_1(x, y)|^2 dx dy \iint |E_0(x, y)|^2 dx dy}}, \quad (1)$$

where E_1 , E_0 are the spatial field distributions of the fundamental and first higher modes of the bi-modal waveguide, respectively. In this equation the tilted Bragg grating is represented by

$$\varepsilon(y, \varphi) = \exp\left(i \frac{2\pi \tan(\varphi)}{\Lambda_z} y\right), \quad (2)$$

with the tilt angle φ , the effective grating period Λ_z along the z -direction (propagation direction) and the width w of the bi-modal waveguide. Finally, the coupling efficiency κ is given by

$$\kappa(\varphi) = \pi Q(\varphi) \frac{\Delta n}{\lambda_B}. \quad (3)$$

Here Δn is the amplitude of refractive index change and λ_B is the Bragg wavelength. Using coupled-mode theory the grating reflectivity R is found to be

$$R(\varphi) = |r(\varphi)|^2 = \tanh^2(\kappa(\varphi)L_g), \quad (4)$$

where L_g is the length of the grating. For a $12\ \mu\text{m}$ wide bi-modal waveguide section, the expected tilt angle for maximum reflection can be estimated to be of the order of one degree.

4 Experimental methods

For waveguide formation crystal samples of $(1 \times 7.8 \times 50)\ \text{mm}^3$ are cut from x -cut LiNbO_3 wafers of congruently melting composition. The ferroelectric c -axis is oriented parallel to the $50\ \text{mm}$ long edge, which is the main propagation direction. To increase the amount of photorefractive centres in the central bi-modal crystal section ($20\ \text{mm}$ long), a $500\ \text{nm}$ thick copper layer is evaporated on the bottom x -facet. The sample is then annealed at $1000\ ^\circ\text{C}$ for $96\ \text{h}$ in air atmosphere for in-diffusion. Following this treatment, the copper concentration is almost constant over the whole crystal thickness. Next, a layer of $100\ \text{nm}$ titanium is evaporated on the top x -facet, opposite to the side that has been evaporated with copper. This procedure leads to a significantly decreased surface roughness that is due to high surface copper concentrations during in-diffusion when compared to single-sided diffusion of both titanium and copper [12]. The in-diffusion of the $100\ \text{nm}$ thick titanium structures takes place at $1000\ ^\circ\text{C}$ for $20\ \text{h}$ in dry air atmosphere. During the last $2\ \text{h}$, wet argon atmosphere is used instead of air to chemically reduce most of the photorefractive centres to Cu^{2+} . Here, we want to note that copper doping does not change the refractive index of LiNbO_3 , thus, the waveguide structures determined by the titanium diffusion profiles are not altered. Several multiplexer structures which differ in inter-waveguide distance b and coupler length L_C are lithographically transferred onto a single sample in order to decrease possible tolerances caused by the adjacent fabrication steps. Other relevant fabrication parameters are described in Sect. 3. Coplanar electrodes are fabricated by evaporating thin gold layers followed by lithographic patterning for electrode separations of $d_0 = 58\ \mu\text{m}$. The electrode structures are shielded on top by a $1\ \mu\text{m}$ thick MgF_2 layer for improved electrical isolation. Finally, the input and output facets of the samples are polished for direct fibre coupling.

The gratings are recorded with a two-beam interference setup using the green light of an argon ion laser at $\lambda = 514.5\ \text{nm}$ [12]. The crystal holder, placed in the interference region of the beams, can be precisely adjusted/rotated relative to the interference fringes to record tilted gratings. For ther-

mal fixing, additional electrical heating elements allow for recording at elevated temperatures of $160\ ^\circ\text{C}$ [15–17]. An active phase stabilisation is utilized to control the interference pattern during grating recording [18].

Here we have to note that when using our two-beam interference set-up and a grating length of $20\ \text{mm}$, the reflectivities are still slightly below one. Furthermore, side lobes of the reflection spectrum may lead to increased cross-talk between adjacent wavelength channels. On the other hand, for application in DWDM, the reflection spectrum of the Bragg grating needs to be almost rectangular, having a flat top and a strong suppression of side lobes at higher/lower wavelengths. Such a performance of the grating can be obtained by using both chirping of the grating period and apodizing, i.e. spatially varying the strength of the grating [19, 20]. In bulk LiNbO_3 crystals, such thermally fixed volume gratings with a flat top region of $0.24\ \text{nm}$ bandwidth (at $-0.5\ \text{dB}$) and $> 25\ \text{dB}$ channel isolation have been obtained [21], e.g. by using adequately designed phase masks for holographic recording [22].

The spectral measurements are performed with the light of an external cavity laser (Tunics Purity) providing tuneable single-longitudinal mode output for wavelengths $\lambda = (1525\text{--}1625)\ \text{nm}$. The polarised light of the laser is coupled either into the input port S_{in} , to the drop port D or to the add port A, respectively, using single-mode polarisation maintaining fibres. An additional polarisation controller allows for selective excitation of either TE or TM modes. Input and output light powers are measured by fibre-coupled photo detectors.

5 Results and discussion

The investigation of mode conversion by the slanted holographic grating is performed in single straight $12\ \mu\text{m}$ wide bi-modal channel waveguides fabricated by diffusion of $100\ \text{nm}$ Ti for $20\ \text{h}$ at $1000\ ^\circ\text{C}$. Elementary holographic gratings with lengths of $L_g = 17\ \text{mm}$ and different tilt angles φ are recorded at room temperature (i.e. without thermal fixing) at fixed conditions. The two recording beams had an intensity of $I = 1.2\ \text{kW}/\text{m}^2$ and the recording time was set to $50\ \text{s}$. A transmission and reflection spectrum is measured immediately after recording in order to avoid any erasure of the grating. The reflectivity R of the grating is evaluated from the transmission spectrum T using the relation $R = 1 - T$. After completion of each measurement, the crystal is illuminated with intense white light for $20\ \text{min}$ to remove the former grating. As an example, in Fig. 2a, a typical trans-

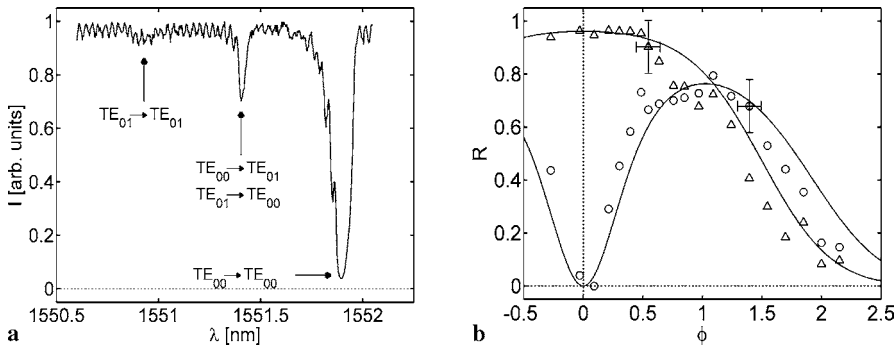


FIGURE 2 (a) Transmission spectrum of a grating tilted by 0.2° : mode conversion (minimum at $1551.4\ \text{nm}$) and simple reflection of fundamental mode (minimum at $1551.8\ \text{nm}$). (b) Reflectivity versus tilt angle φ . Both fundamental mode reflection (Δ) and mode conversion (o) of fundamental into first higher mode are depicted. The solid line plots the theoretical reflectivity $R(\varphi)$ using (4) with refractive index amplitude $\Delta n = 6.7 \times 10^{-5}$ and grating length $L_g = 17\ \text{mm}$

mission spectrum for a tilt angle $\varphi = 0.2^\circ$ is shown. The peak positions at wavelengths λ_B are a result of the generalized Bragg condition $\lambda_B = \Lambda_z(n_{\text{eff},\text{in}} + n_{\text{eff},\text{refl}})$, where $n_{\text{eff},\text{in}}$ and $n_{\text{eff},\text{refl}}$ are the effective refractive indices of incident and reflected light, respectively. The strongest minimum at a wavelength of 1551.9 nm is related to the direct reflection of the fundamental mode without mode conversion. The second (weaker) minimum at the wavelength 1551.4 nm shows the two (degenerate) reflections of the fundamental mode into the first higher mode, and vice versa. The direct reflection of the only weakly excited higher mode is expected to occur at a wavelength of 1550.9 nm, but is hardly visible. To further suppress this process, the input optical fibre is precisely aligned for maximum in-coupling efficiency. In Fig. 2b the measured reflectivity $R(\varphi)$ for the reflection (of the fundamental mode) as well as for the mode conversion (from fundamental to backwards-propagating higher mode) process are shown as a function of tilt angle φ . As can be seen, the maximum of mode conversion is obtained at $\varphi = (1.0 \pm 0.1)^\circ$, which is in good agreement with the theoretical dependence where a refractive index amplitude Δn of 6.7×10^{-5} has been used for fitting. However, at this tilt angle, a rather large reflectivity of the fundamental mode itself is obtained. This undesired reflection is a consequence of the simple tilted elementary grating used. A strong reduction of this effect may be achieved by using more sophisticated grating shapes, e.g. an asymmetric or segmented grating profile adapted to the transverse phase profile of the higher mode in y -direction [23, 24]. Here, we also want to note that the limited maximum reflectivity of the higher mode ($\sim 80\%$) is due to the rather short recording time (50 s) of the Bragg grating, but can be easily increased to values close to one for longer record-

ing. Alternatively, a longer grating length can be used as well.

For the measurement of the performance of the add/drop multiplexer, thermally fixed gratings are recorded under the optimal tilt angle $\varphi = 1.0^\circ$ in the bi-modal section of complete multiplexer structures. Here, recording times are 2 h with the same intensity $I = 1.2 \text{ kW/m}^2$ as before. In Fig. 3, transmission spectra of all four ports of an add/drop multiplexer designed for the wavelength $\lambda_B = 1555.7 \text{ nm}$ are shown. In Fig. 3a, TE polarized light is inserted at S_{in} . In the first spectrum (I) obtained at S_{in} , a strong reflection of the fundamental mode at $\lambda = 1556.2 \text{ nm}$ can be seen, superimposed by a larger background that is mostly due to Fabry–Pérot oscillations between crystal facets as well as between crystal input facet and optical fibre. This undesired noise may be mostly suppressed in a later device by polishing the end facets of the crystal under a certain angle. Figure 3a-II shows the spectrum measured at port D. Obviously, only the reflected, mode-converted higher mode leave the device at this port, pointing to a reflectivity close to one at $\lambda = 1555.7 \text{ nm}$ for drop operation of the multiplexer. The broadening of the peak to shorter wavelengths is probably attributed to the Fabry–Pérot cavity formed by the crystal facets and the grating [6]. In the next row in Fig. 3a-III, the transmission spectrum measured at S_{out} is given. Both reflection and mode conversion peaks show high diffraction efficiencies, the latter being about 96%. To monitor cross-talk of the device the logarithmic plot of the drop port spectrum in Fig. 3a-IV (taken from the data in part II) is used, which shows a suppression of the neighboured self-reflection of the fundamental mode of more than 22 dB. Cross-talk from the next data channel at $\pm 0.8 \text{ nm}$ distance is reduced by about 30 dB. These values are in good agreement with numerical

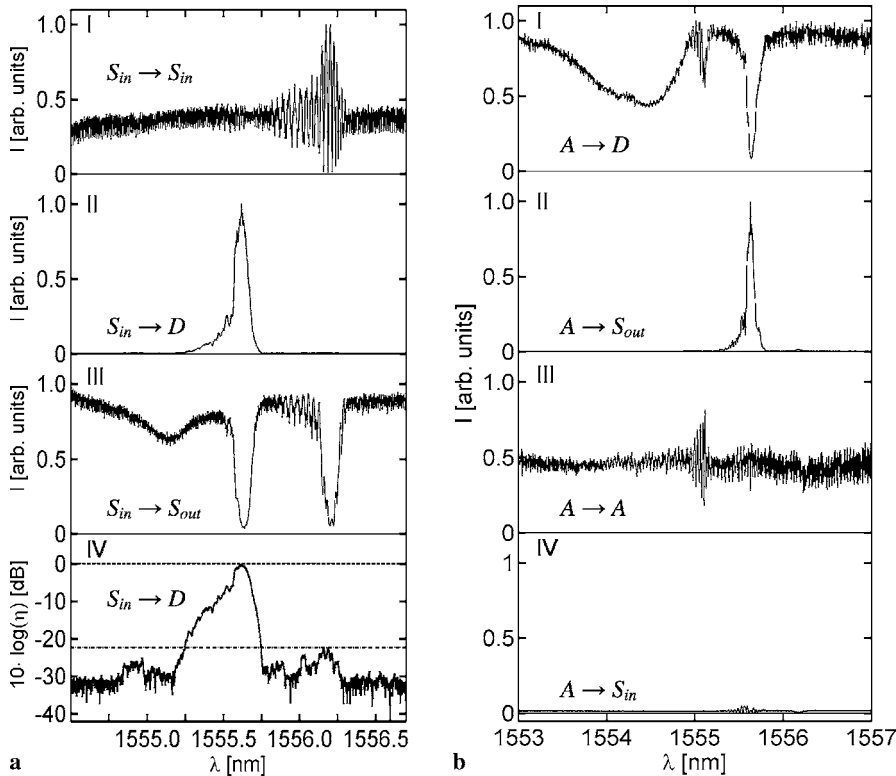


FIGURE 3 (a) Optical intensity spectra for TE polarized light insertion at input port S_{in} . I, simple reflection of the incoming light measured at S_{in} ; II, spectrum measured at port D; III, transmitted light at S_{out} ; IV, logarithmic plot of the dropped light of II with $\eta = I/I_0$, where I_0 is incident light intensity. (b) Spectra for light insertion at the add port A. Measured spectrum at D (I), S_{out} (II), A (III), and at S_{in} (IV)

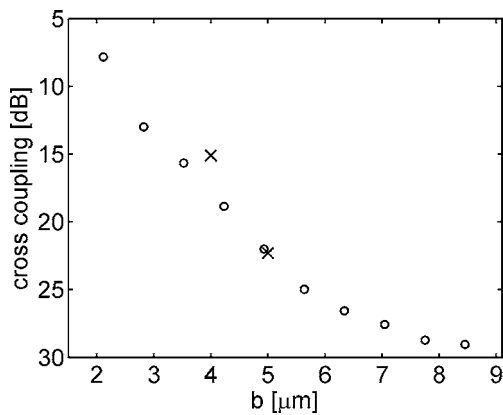


FIGURE 4 Simulated (o) and measured (x) cross-talk as a function of the inter-waveguide distance b and for TE polarized light

data obtained by BPM simulations of the multiplexer. Some measured and calculated values of cross-talk as a function of inter-waveguide distance b are given in Fig. 4.

Next, in order to verify the add operation, light is inserted at the add port A in Fig. 3b. For this situation, the transmission spectrum is measured at port D. The most pronounced transmission dip in Fig. 3b-I is due to mode conversion from the first higher mode (that is excited via the directional coupler) into the fundamental mode, while this converted mode is directed to port S_{out} [see Fig. 3b-II]. The direct reflection of the higher mode (smaller dip in Fig. 3b-I at $\lambda \approx 1555.1$ nm) couples back to the add port A and is monitored in Fig. 3b-III. The undesired transmission from A to S_{in} , where the added signal propagates in the opposite (wrong) direction, is shown in Fig. 3b-IV. Only a weak signal is measured, which at least partly originates from light reflection at the end facet at S_{out} . Again, this signal can be suppressed by polishing the facets used for light coupling at a certain angle.

For electrical tuning and switching, coplanar electrodes are placed on the substrate, enclosing the bi-modal waveguide section (see Fig. 1). In Fig. 5, the polarisation dependence for different bias fields is depicted. The hardly avoidable small mismatch of propagation constants of TE and TM polarised modes (refer to spectra for 0 kV/mm), which may occur due to fabrication tolerances even for optimized waveguide geometries, leads to a small difference (gap) of corresponding Bragg wavelengths but vanishes under the influence of an electric field of $E = 2.3$ kV/mm (corresponding to an applied voltage of $U = \pi d_0 E = 420$ V, however, this voltage may be significantly decreased by using smaller electrode separations). Presently, we have made use of the fact that the relevant electro-optic tensor elements $r_{12} = -r_{22}$ of the two ordinarily polarized modes have equal magnitudes but opposite signs. Swapping the electric field direction doubles the gap size and thus allows for fast switching operation. In the case of a multiplexer designed for the channel wavelength $\lambda = 1555.38$ nm (dotted vertical line), the multiplexer can be turned on (positive voltage) and off (negative voltage) by applying the electric fields $E = \pm 2.3$ kV/mm.

The insertion loss of the device strongly depends on the copper concentration in the grating section. For undoped multiplexer structures, losses of only 0.6 dB are measured. Copper concentrations of about $4.7 \times 10^{25} \text{ m}^{-3}$ in the 20 mm long

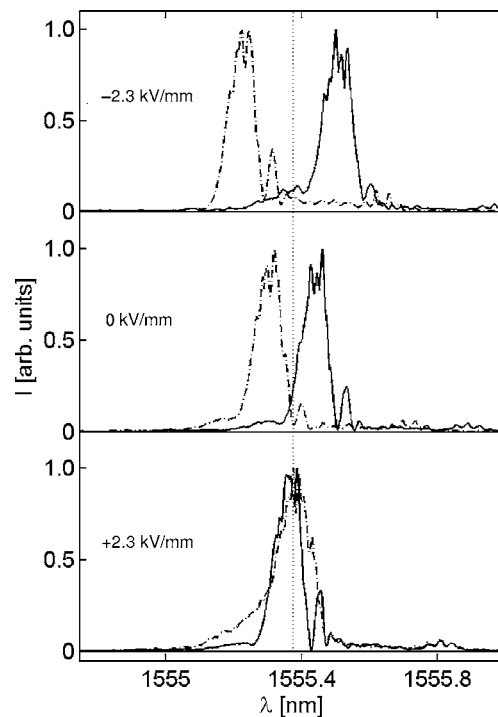


FIGURE 5 Shift of Bragg wavelength due to bias electrical field. Spectra are measured at D after light insertion at S_{in} . The undesired mismatch between TE (solid line) and TM (dash-dotted line) polarisations can be compensated using a bias field of 2.3 kV/mm. Swapping of the field polarity is used for on/off switching of the filter that is designed for wavelength channel $\lambda = 1555.38$ nm (dotted vertical line)

bi-modal waveguide section result in loss values of 4.6 dB due to surface scattering and residual absorption. Further development of the fabrication process as well as using iron doping, which usually shows lower damping at 1.5 μm wavelengths [25], instead of copper may decrease these losses significantly.

6 Conclusions

An integrated-optical add/drop multiplexer in lithium niobate for the infrared wavelength region around 1.5 μm is demonstrated. The Bragg reflection of the tilted grating is measured to be 96% and may further be increased by means of longer gratings. A still moderate insertion loss of 4.6 dB is obtained for copper-doped samples, whereas undoped samples show a minimum loss of only 0.6 dB. Both the measured and calculated channel rejections for nonresonant channels are above 22 dB.

ACKNOWLEDGEMENTS We would like to thank the Deutsche Forschungsgemeinschaft for the financial support of this research (DFG KI482/6-1 and 6-2).

REFERENCES

- 1 S.V. Kartalopoulos, *DWDM: Networks, Devices, and Technology* (Wiley-Interscience, Hoboken, NJ, 2003)
- 2 C.R. Giles, *J. Lightw. Technol.* **15**, 1391 (1997)
- 3 A.V. Tran, W.D. Zhong, R.C. Tucker, R. Lauder, *IEEE Photon. Technol. Lett.* **13**, 582 (2001)
- 4 K. Okamoto, K. Takiguchi, Y. Ohmori, *Electron. Lett.* **31**, 723 (1995)
- 5 F. Bilodeau, D.C. Johnson, S. Theriault, B. Malo, J. Albert, K.O. Hill, *IEEE Photon. Technol. Lett.* **7**, 388 (1995)

- 6 T. Erdogan, J.E. Sipe, *J. Opt. Soc. Am. A* **13**, 296 (1996)
- 7 A.S. Kewitsch, G.A. Rakuljic, P.A. Wilems, A. Yariv, *Opt. Lett.* **23**, 106 (1998)
- 8 H.S. Park, S.H. Yun, I.K. Hwang, S.B. Lee, B.Y. Kim, *IEEE Photon. Technol. Lett.* **13**, 460 (2001)
- 9 D.F. Geraghty, D. Provenzano, M.M. Morrell, S. Honkanen, A. Yariv, N. Peyghambarian, *Electron. Lett.* **37**, 829 (2001)
- 10 J.M. Castro, D.F. Geraghty, B.R. West, S. Honkanen, *Appl. Opt.* **43**, 6166 (2004)
- 11 R. Asquini, J. D'Angelo, A. d'Alessandro, *Molecular Cryst. Liquid Cryst.* **450**, 403 (2006)
- 12 J. Hukriede, D. Runde, D. Kip, *J. Phys. D Appl. Phys.* **72**, R1 (2003)
- 13 D. Runde, S. Breuer, D. Kip, submitted to *J. Lightw. Technol.*
- 14 J. Hukriede, I. Nee, D. Kip, E. Krätzig, *Opt. Lett.* **23**, 1405 (1998)
- 15 J. Hukriede, D. Kip, E. Krätzig, *Appl. Phys. B* **72**, 749 (2001)
- 16 K. Buse, S. Breer, K. Peithmann, S. Kapphan, M. Gao, E. Krätzig, *Phys. Rev. B* **56**, 1225 (1997)
- 17 J. Hukriede, D. Kip, E. Krätzig, *Appl. Phys. B* **66**, 333 (1998)
- 18 P.M. Garcia, K. Buse, D. Kip, J. Frejlich, *Opt. Commun.* **117**, 235 (1995)
- 19 M. Matsuhara, K.O. Hill, *Appl. Opt.* **13**, 2886 (1974)
- 20 P.S. Cross, H. Kogelnik, *Opt. Lett.* **1**, 43 (1977)
- 21 C. Moser, F. Havermeier, W. Liu, G. Steckman, K. Buse, D. Psaltis, *Proc. OFC 2003* (2003), pp. 644–645
- 22 J. Albert, K.O. Hill, B. Malo, S. Thériault, F. Bilodeau, D.C. Johnson, L.E. Erickson, *Electron. Lett.* **31**, 222 (1995)
- 23 T. Erdogan, *Opt. Commun.* **157**, 249 (1998)
- 24 J.M. Castro, D.F. Geraghty, S. Honkanen, C.M. Greiner, D. Iazikov, T.W. Mossberg, *Opt. Express* **13**, 4180 (2005)
- 25 S. Breer, H. Vogt, I. Nee, K. Buse, *Electron. Lett.* **34**, 2419 (1999)